HAMAMATSU
PHOTON IS OUR BUSINESS

FTIR engine

Contents

1. Overview

The Fourier transform infrared spectrometer (FTIR) engine is compact enough to carry in just one hand. A Michelson optical interferometer and control circuit are built into a palm-sized enclosure. Spectrum and absorbance can be measured by connecting a PC via USB. It can be applied to real-time measurement performed on site without bringing the measurement sample into the analysis room as well as continuous monitoring.

The FTIR engine's optical interferometer has a movable mirror (ϕ3 mm) that uses Micro Electro Mechanical Systems (MEMS) technology and a fixed mirror. The built-in semiconductor laser (VCSEL: vertical cavity surface emitting laser) for monitoring the movable mirror position allows spectrum measurement with high wavelength accuracy. The product includes evaluation software with functions for setting measurement conditions, acquiring and saving data, drawing graphs, and so on. Furthermore, the dynamic link library (DLL) function specifications are disclosed, so users can create their original measurement software programs.

2. Structure

The FTIR has the following features compared to the dispersive type (diffraction grating type) spectrometer.

- High S/N because simultaneous signal measurements are possible in the entire spectral range
- High light utilization efficiency if the resolution is the same as the dispersive type spectrometer since the incident hole can be enlarged
- High wavelength accuracy and reproducibility because laser wavelength is used for calibration

The FTIR's optical interferometer is composed of a light input section, beam splitter (semi-transparent mirror), fixed mirror, ϕ3 mm movable mirror, photodetector, and so on. The incident light is split into two light beams, transmitted light and reflected light, by a beam splitter. The two light beams are reflected by the fixed mirror and movable mirror and return to the beam splitter, where they are recombined, causing optical interference. The photodetector acquires light intensity signals that varies depending on the movable mirror position. The optical spectrum is obtained by taking the Fourier transform of this light intensity signal.

An optical fiber is connected to the connector at the light input section of the FTIR engine. Light from the measurement sample can be input to the FTIR engine through an optical fiber, which provides a highly flexible measurement system.

[Figure 2-1] FTIR configuration and operating principle

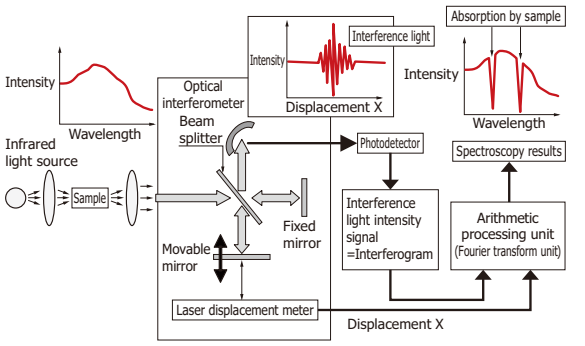

KACCC0714EB

2 - 1 Movable mirror

The FTIR engine has a built-in electrostatically driven movable mirror [Figure 2-2]. When a voltage is applied to the comb electrodes, an electrostatic driving force is generated. As a result, the torsion bars twist causing the beams to move, and the movable mirror moves vertically in parallel. The movable mirror moves by a great amount when driven at the resonant frequency.

[Figure 2-2] Movable mirror and electrostatic actuator

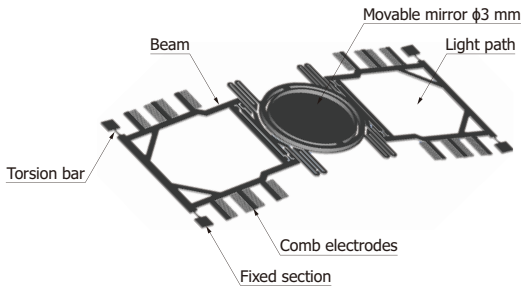

KACCC1006EA

2 - 2 Optical interferometers

Figure 2-3 (a) shows a typical interferometer used in an FTIR, and Figure 2-3 (b) shows the interferometer used in the FTIR engine. The optical interferometer is composed of a light input section, beam splitter, fixed mirror, movable mirror, photodetector, and so on. Using a wavelength dispersion compensator made of the same material as the beam splitter, a fixed mirror is formed on the back side. The optical interferometer is designed so that the optical path difference between the movable mirror side and fixed mirror side is zero at the position where the movable mirror has moved about 70 µm (thickness of the movable mirror) below the position of the movable mirror in Figure 2-3 (b).
The optical interferometer has a built-in MEMS chip shown in Figure 2-4. The MEMS chip is resin-sealed in a package [Figure 2-5]. It prevents the entry of fine particles, but moisture is permeable. Make sure condensation does not form on the beam splitter, lens, or movable mirror, as condensation may degrade the characteristics.

[Figure 2-3] Optical interferometer

(a) FTIR interferometer

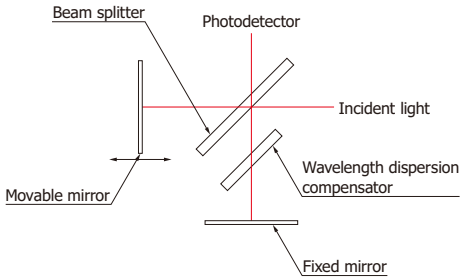

KACCC1007EA

(b) FTIR engine interferometer

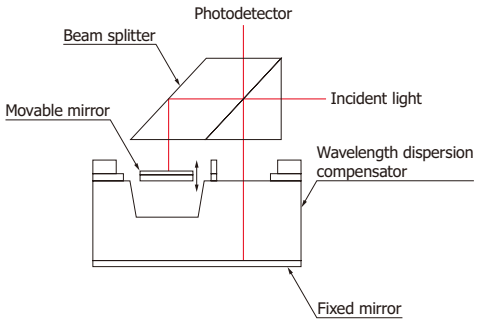

KACCC1008EA

[Figure 2-4] MEMS chip (built into the optical interferometer)

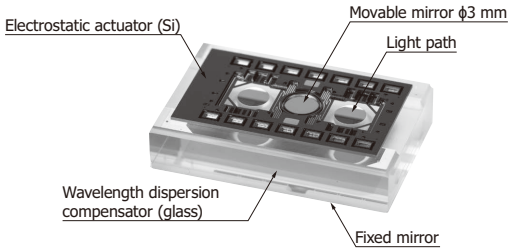

KACCC1009EA

» Structure

Figure 2-5 shows the optical system of the FTIR engine. There are two interferometers in the FTIR engine: infrared interferometer and laser interferometer. The infrared interferometer measures the near infrared light input from the optical fiber, and the laser interferometer monitors the movable mirror position using a semiconductor laser (VCSEL). The positions of the two optical interferometers

are separated by a dichroic mirror. An InGaAs PIN photodiode (G12183-003K) is used for the infrared interferometer's photodetector and a Si PIN photodiode (S5821-03) for the laser interferometer's photodetector.

[Figure 2-5] Optical system of FTIR engine

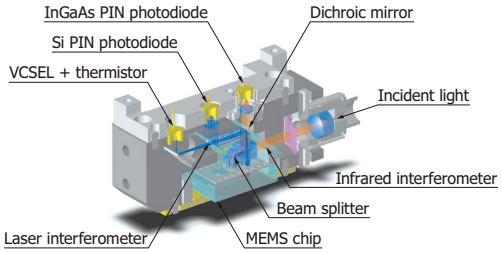

KACCC1010EA

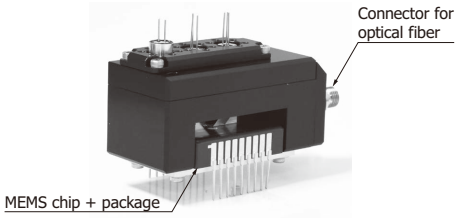

KACCC1011EA

2 - 3 Control circuit

Figure 2-6 shows the block diagram of the FTIR engine. The control circuit consists of an analog controller, digital controller, and external interface. The power is supplied through the USB bus from the PC. The analog controller drives the movable mirror and VCSEL and amplifies the optical signal from the photodetector. The preamp amplifies the optical signal. The gain can be switched between five levels. The amplified optical signals are converted into digital signals by the A/D converter and sent to the digital controller. The field-programmable gate array (FPGA) of the digital controller configures the analog controller and controls the drive timing and data acquisition timing. The FPGA also performs optical signal integration in sync with the drive timing. The external interface contains a microcontroller unit (MCU) and connects to a PC via a USB cable. The MCU receives the control signals from the PC and sends the optical signal data from the two photodetectors to the PC.

[Figure 2-6] Block diagram

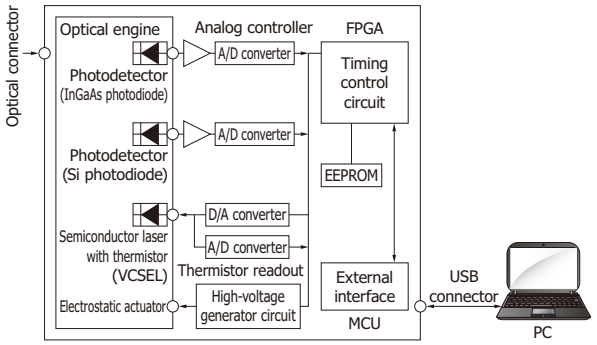

KACCC1012EA

2 - 4 Software

The FTIR engine is equipped with a USB interface (USB 2.0), which is used to connect to the PC. By using the DLL, you can drive the movable mirror, set measurement conditions (gain, integration count, etc.), start a measurement, acquire data, and so on. The optical signals acquired by the two photodetectors are each integrated by the FPGA and sent to the PC. On the PC, the optical interference signal necessary to obtain the optical spectrum is calculated, and Fourier transform is taken. The supplied CD-ROM contains evaluation software and DLL as well as sample code that you can use to create your own measurement software [Figure 2-7].

[Figure 2-7] Software configuration

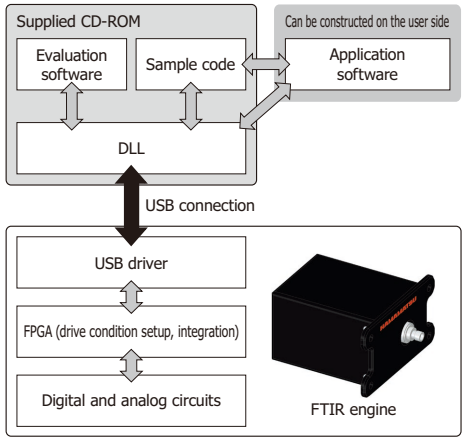

KACCC1013EA

3. Operating principle

3 - 1 Movable mirror

The movable mirror drive conditions are stored in the EEPROM of the control circuit. The movable mirror can be driven in resonance by reading information from the EEPROM.
The electrostatic actuator that drives the movable mirror can be represented by the dynamic model in Figure 3-1. The spring constant is mainly determined by the Young's modulus and Poisson's ratio of the spring material and the spring shape (length, thickness, width). The spring is formed with high accuracy by applying semiconductor lithography technology and etching technology, but there are some variations in the spring dimensions and spring constant. Therefore, the drive frequency of the movable mirror varies by product.

[Table 3-1] Electrical characteristics (drive frequency) of movable mirror

Parameter	Min.	Typ.	Max.	Unit
Drive frequency	225	275	325	Hz

[Figure 3-1] Dynamic model of electrostatic actuator

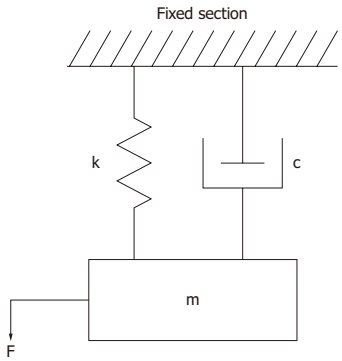

k : spring constant
c : viscosity
m: weight
F : electrostatic driving force

KACCC1014EA

The spring characteristic of an electrostatic actuator has a non-linear characteristic called hardening, and the movable mirror's amplitude changes drastically at a specific drive frequency. This is shown by the duffing equation [Equation (3-1)]. In the range where the amplitude changes drastically, the characteristics differ from low frequency to high frequency and from high frequency to low frequency. In the range where the characteristics are the same, a stable amplitude can be obtained by setting the drive frequency [Figure 3-2].

$$m\ddot{x} + c\dot{x} + (1 + \beta x^2)kx = F\cos(wt) \cdots\cdots (3\text{-}1)$$

[Figure 3-2] Amplitude vs. drive frequency (typical example)

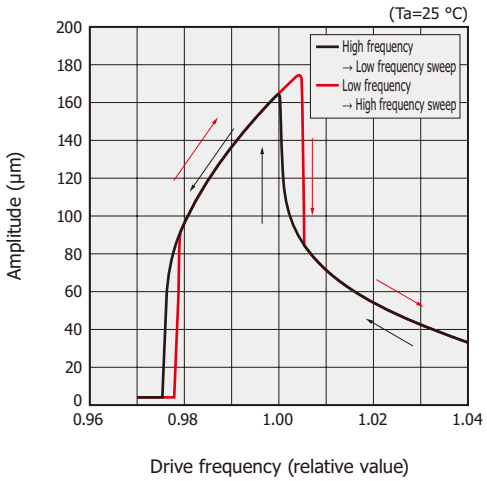

KACCB0594EA

The natural frequency of a movable mirror is expressed by equation (3-2). The resonant frequency of the movable mirror that has a non-linear spring shifts according to the amplitude [Equation (3-3)]. When the amplitude of the movable mirror increases due to hardening, the spring constant increases, which increases the resonant frequency [Figure 3-3].

$$\omega_0 = \sqrt{\frac{k}{m}} \cdots\cdots (3\text{-}2)$$

ω_0: natural frequency
m : weight
k : spring constant

$$\omega_1 = \omega_0 \sqrt{1 + \frac{3}{4}\beta x^2} \cdots\cdots (3\text{-}3)$$

ω_1: resonant frequency
β : non-linearity constant of spring
x : amplitude

The electrostatic driving force of the movable mirror is expressed by equation (3-4).

$$F = \frac{1}{2}\frac{dC}{dx}V^2 \cdots\cdots (3\text{-}4)$$

F: electrostatic driving force
C: capacitance of comb electrodes (composed of multiple parallel plates)
V: drive voltage

[Figure 3-3] Drive frequency characteristics (typical example)

(a) Amplitude vs. drive frequency

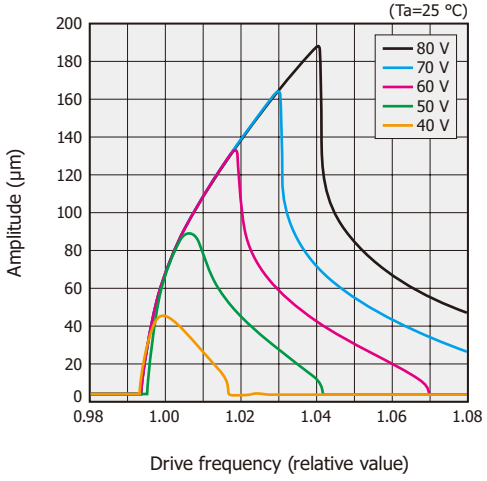

KACCB0595EA

(b) Maximum amplitude vs. drive frequency

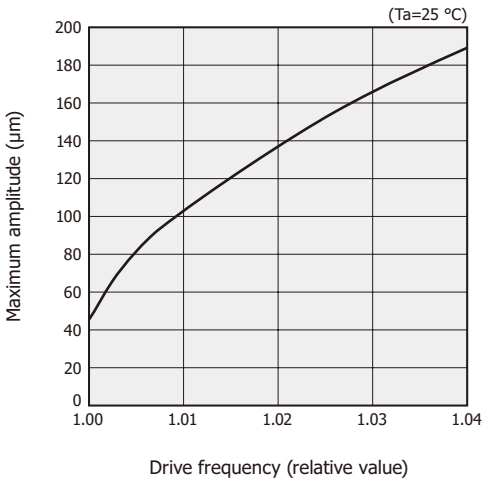

KACCB0596EA

Since the movable mirror spring is made of single-crystal silicon, it has the advantage of low metal fatigue and long life. As the temperature increases, the Young's modulus of the single-crystal silicon decreases. Therefore, when the temperature changes, the spring constant changes, which causes the movable mirror's resonant frequency to change [Figure 3-4].

[Figure 3-4] Temperature characteristics of drive frequency (typical example)

(a) Amplitude vs. drive frequency

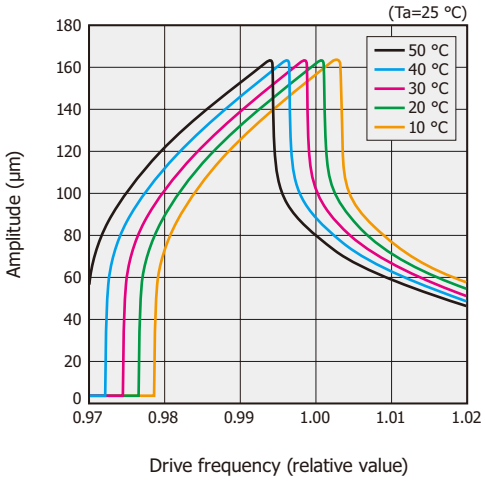

KACCB0597EA

(b) Drive frequency vs. ambient temperature

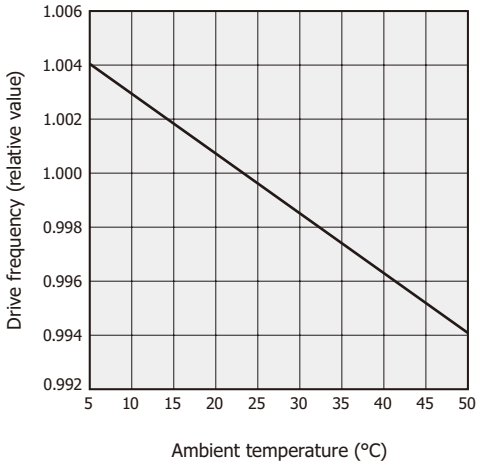

KACCB0598EA

Control method

The FTIR engine stores the optimum conditions in EEPROM in order to stably drive the movable mirror. In addition, the thermistor embedded in the FTIR engine enclosure measures the temperature, and the optimal drive frequency is set according to the temperature change. Figure 3-5 shows the temperature characteristics of the movable mirror's drive frequency and amplitude.

[Figure 3-5] Temperature characteristics of drive frequency and amplitude (typical example)

(a) Drive frequency vs. temperature

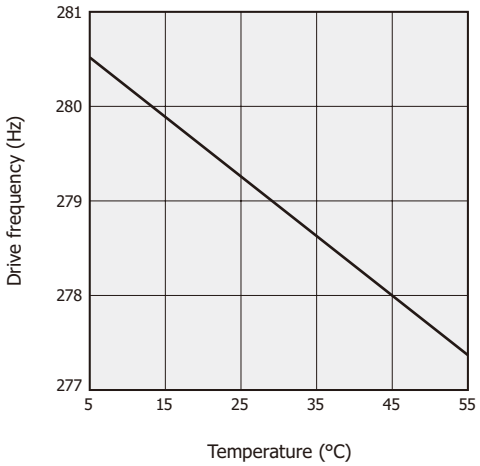

KACCB0599EA

(b) Amplitude vs. temperature

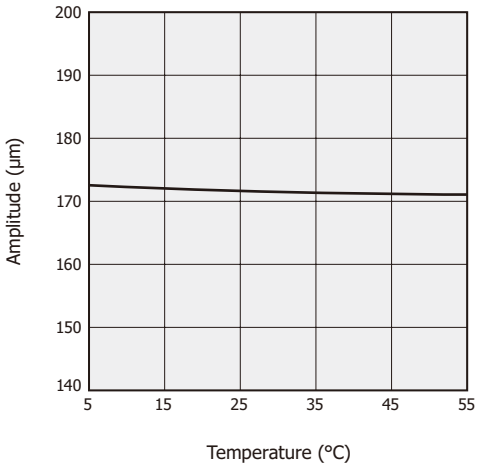

KACCB0600EA

3 - 2 Optical interferometers

The photocurrent obtained by inputting light to the optical interferometer (infrared interferometer, laser interferometer) is expressed by equation (3-5). The AC component in the second term of equation (3-5) is an optical interference signal called an interferogram. At the position where the optical path difference between the movable mirror and fixed mirror is zero, the light of each wavelength interferes with each other, which increases the optical interference signal. As the distance from the zero optical path difference increases, the light of each wavelength interferes at various positions, which causes a decreasing ripple [Figure 3-6]. This optical interference signal can be Fourier transformed to obtain the optical spectrum.

$$I(x) = \int_0^\infty B(v)(1 + \cos 2\pi vx)dv \quad \cdots\cdots\cdots\cdots \quad (3\text{-}5)$$

I(x) : photocurrent
B(v): optical spectrum
V : wavenumber
X : optical path difference

[Figure 3-6] Optical interference signal

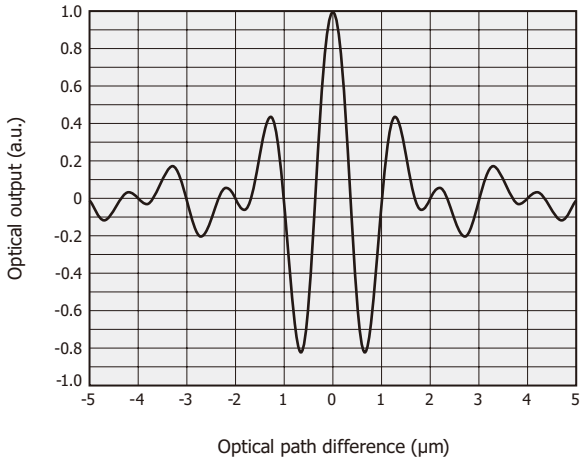

KACCB0601EA

The wavenumber resolution of the FTIR is defined by wavenumber Δv (unit: cm^{-1}), which is the reciprocal of the wavelength of light. The wavenumber resolution is determined by the movable mirror's amplitude, the light beam's spread angle in the optical interferometer, the movable mirror's tilt, and so on [Figure 3-7].
The wavenumber resolution is expressed by equation (3-6) and improves as the movable mirror's amplitude increases.

$$\Delta v = \frac{1}{4L_1} \quad \cdots\cdots\cdots\cdots \quad (3\text{-}6)$$

Δv: wavenumber resolution
L_1 : amplitude

The effect of the light beam's spread angle is expressed by equation (3-7).

$$\Delta v = \left(\frac{df}{2f}\right)^2 v \quad \cdots\cdots\cdots\cdots \quad (3\text{-}7)$$

df: diameter of input optical fiber
f : focal distance of incident lens
v : wavenumber [cm^{-1}]

[Figure 3-7] Lens and light beam

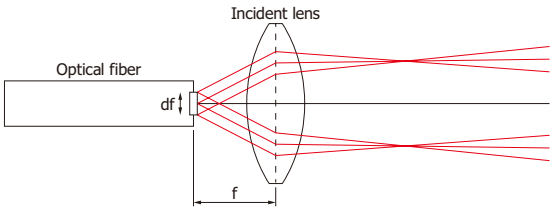

KACCC1015EA

Wavenumber resolution (unit: cm^{-1}) can be converted to spectral resolution (unit: nm) [Equation (3-8)]. The spectral resolution varies depending on the wavelength and degrades at longer wavelengths. Figure 3-8 shows a typical example of the measured wavelength resolution.

$$\Delta\lambda = \left(\frac{1}{v} - \frac{1}{v + \Delta v}\right) \times 10^7 \quad \cdots\cdots\cdots\cdots \quad (3\text{-}8)$$

Δλ: spectral resolution

[Figure 3-8] Spectral resolution vs. wavelength (typical example, FWHM)

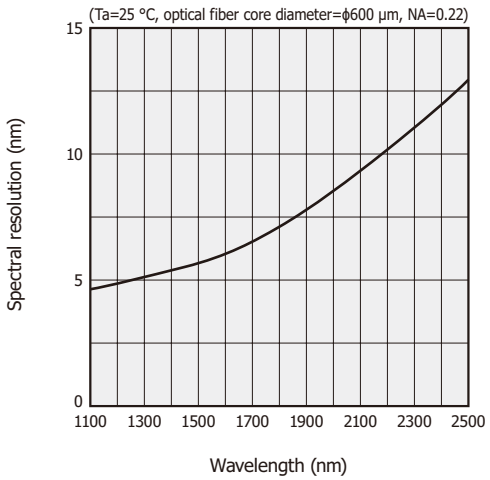

KACCB0602EA

Table 3-2 shows the optical specifications of the FTIR engine.

[Table 3-2] Optical specifications

Parameter	Condition	Typ.	Unit
Optical input connector		SMA connector for optical fiber	-
Incident lens focal distance	λ=1150 nm	6.24	mm
Incident lens NA		0.4	-
Spectral resolution (FWHM)	λ=1532 nm	5.7	nm

» Zero fill processing

One method of smoothing the acquired optical spectrum is zero fill processing [Figure 3-9]. This is a process of adding zeros at each end of the optical interference signal before the Fourier transform, which allows interpolation between points plotted after the Fourier transform. The resolution does not change in this case.

[Figure 3-9] Zero fill processing

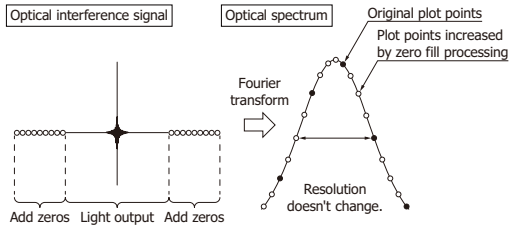

KACCC1016EA

3 - 3 Control circuit

The FPGA of the digital controller drives the movable mirror and controls the measurement timing. The movable mirror is driven when the built-in high voltage IC (HVIC) applies a square-wave drive voltage to the comb electrodes. The number of times the drive voltage is applied from when driving is started is counted.

The optical signals detected by the infrared interferometer and laser interferometer are amplified by the preamplifier and then converted to 16-bit digital signals by two A/D converters whose sampling timing is synchronized.

[Table 3-3] Electrical characteristics

Parameter	Typ.	Unit
A/D resolution	16	bit
A/D sampling rate	140	ns

The FTIR engine measurement starts when the drive voltage of the movable mirror is input. Data is acquired for the specified number of cycles, and the acquired optical signals are integrated in the FPGA [Figure 3-10]. The measurement data is defined by using the “0” or “1” of the least significant bit (LSB) according to the movable mirror’s vertical movement. The relationship between the movable mirror’s vertical movement and the “0” and “1” of the least significant bit changes each time drive start is set.

[Figure 3-10] Timing chart (Direction=1, Cycle=2)

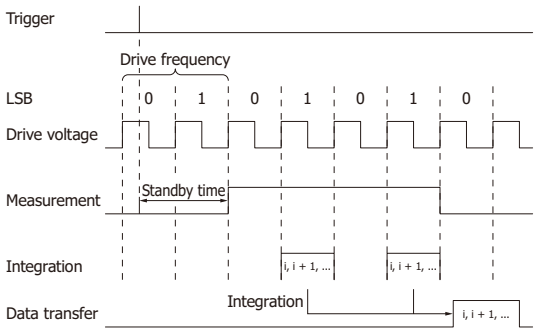

KACCC1017EA

The deviation between the phases of the movable mirror and the drive voltage decreases as the frequency approaches the resonant frequency, and the phases match at the resonant frequency. At the resonant frequency, the mirror amplitude changes drastically as shown in Figure 3-2, making it difficult to control. The drive frequency under the FTIR engine’s recommended operating conditions is lower than the resonant frequency. As a result, a phase shift occurs between the movable mirror and the drive voltage [Figure 3-11]. Due to the phase shift, the digital data of the control circuit is valid up to the amplitude peak and invalid after the peak in Figure 3-11.

[Figure 3-11] Amplitude and drive voltage of movable mirror (typical example)

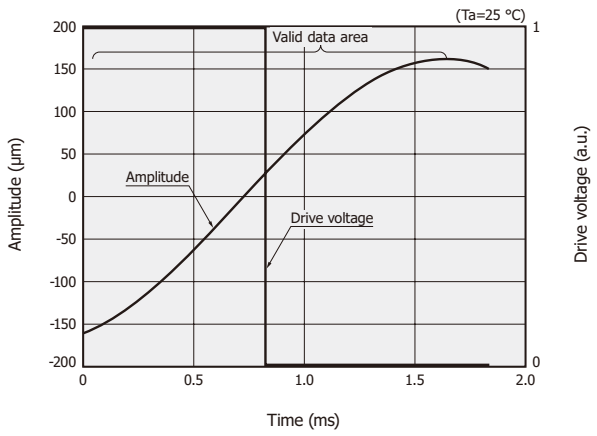

KACCB0663EA

Figures 3-12 and 3-13 show the digital data measured by the infrared interferometer and laser interferometer.

[Figure 3-12] Digital data of infrared interferometer and laser interferometer (measurement example, Direction=0)

(a) Digital data

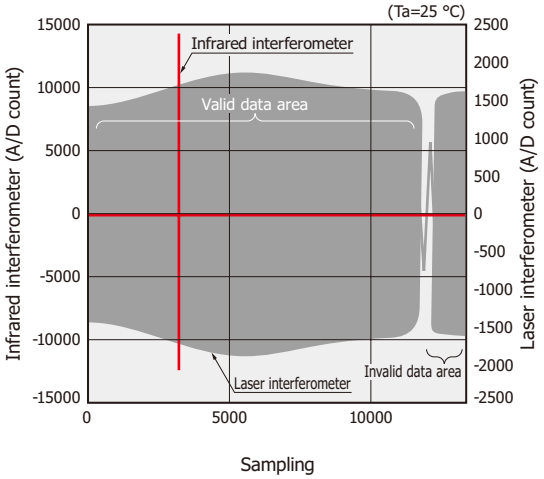

KACCB0604EA

(b) Enlarged view near zero optical path difference

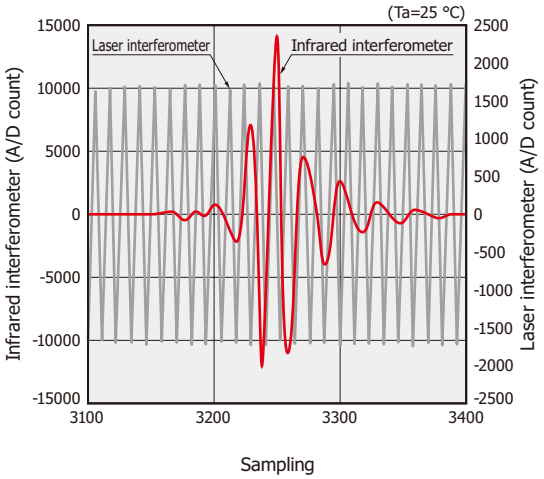

KACCB0605EA

[Figure 3-13] Digital data of infrared interferometer and laser interferometer (measurement example, Direction=1)

(a) Digital data

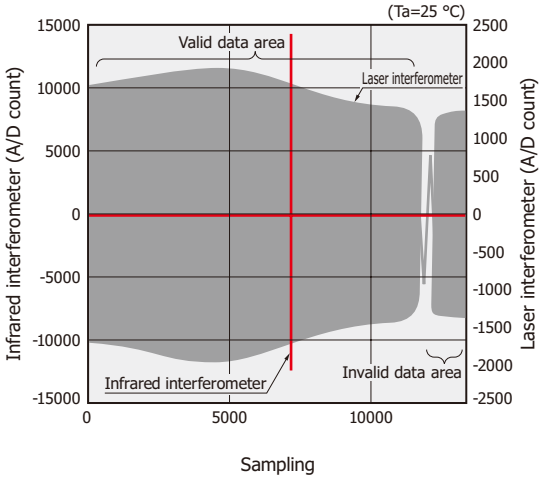

KACCB0606EA

(b) Enlarged view near zero optical path difference

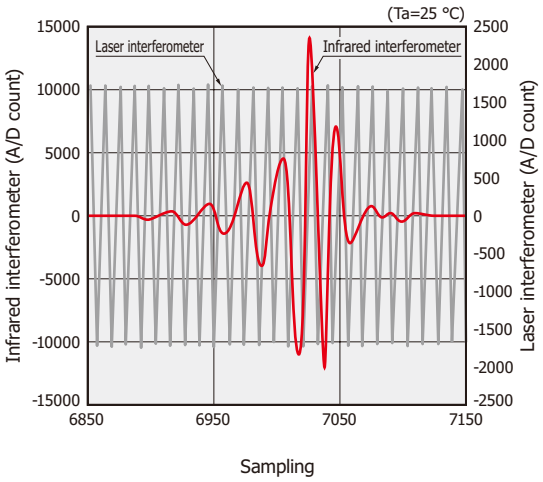

KACCB0607EA

3 - 4 Measurement flowchart

The FTIR engine performs data communication with the PC over a USB 2.0 connection. Figure 3-14 shows the measurement flowchart. For details, refer to the DLL and sample code in the supplied CD-ROM.
Stable measurement using the FTIR engine is achieved by the thermistor measuring the internal temperature of the FTIR engine and waiting until the temperature stabilizes. It is recommended to perform reference measurement and sample measurement under the same movable mirror drive conditions and measurement conditions.

[Figure 3-14] Measurement flowchart

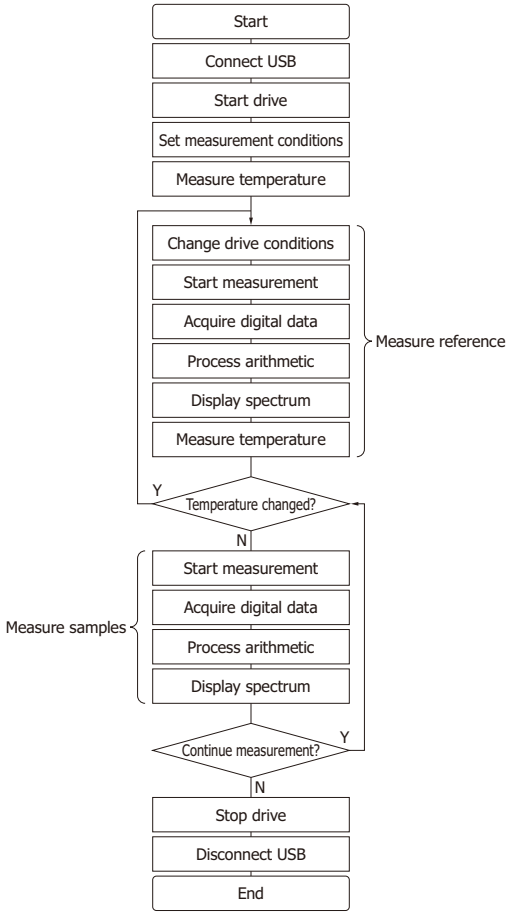

KACCC1018EA

4. Characteristics

4 - 1 S/N

The FTIR engine's signal-to-noise ratio (S/N) is defined as the ratio between the maximum value of the optical spectrum and the effective noise value (RMS) when halogen light is incident. The light source output needs to be adjusted or an ND filter needs to be used to obtain an appropriate incident light level to prevent the FTIR engine's A/D converter from saturating. Since the FTIR engine uses 16-bit A/D converters, adjust the incident light level so that the optical interference signal is between 40000 and 64000 counts p-p. The incident light level needs to be adjusted for each product as the sensitivity differs by product [Figure 4-2].

[Figure 4-1] S/N measurement system

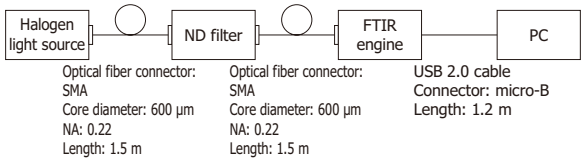

KACCC1019EA

[Figure 4-2] Incident light level adjustment

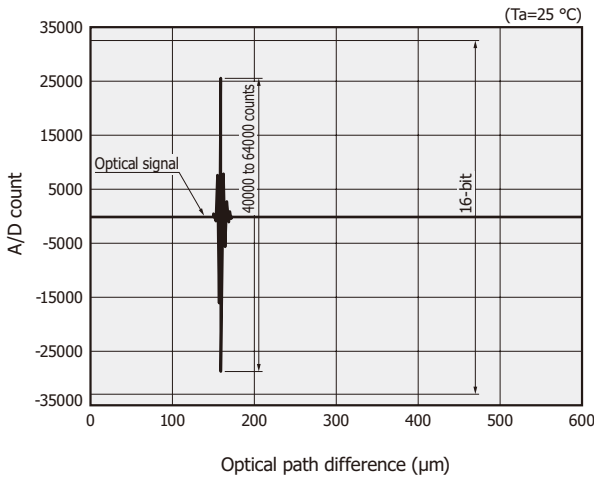

KACCB0608EA

Table 4-1 shows a typical example of the S/N characteristics in the measurement system of Figure 4-1. The S/N is 10000 or more at a gain setting between 1 and 4. The lower the gain, the lower the noise and the higher the S/N.

[Table 4-1] S/N characteristics (typical example, Ta=25 °C, halogen light source, optical fiber core diameter: 600 µm, NA: 0.22, integration count: 512, optical interference signal: approx. 40000 counts p-p)

Gain setting	Gain typ.	S/N typ.
0	526400	7500
1	246400	15000
2	112000	30000
3	52640	45000
4	24640	55000

Figure 4-3 shows the optical spectrum when the light from the halogen light source is incident and the noise spectrum in the dark state. The optical spectrum near 1900 nm is the highest, and the S/N is also high.

[Figure 4-3] S/N characteristics (measurement example)

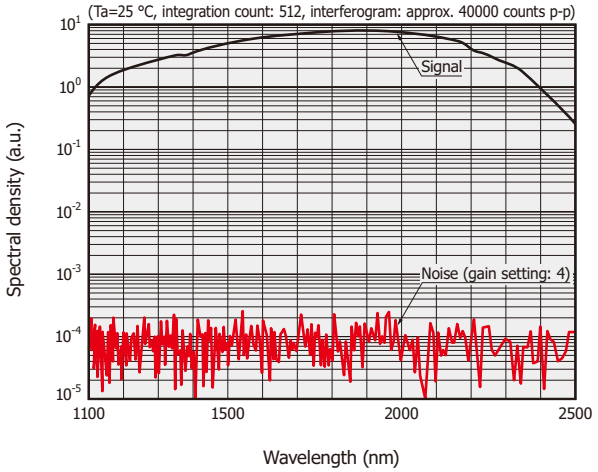

KACCB0609EA

Figure 4-4 shows the relationship between the effective value (RMS) of the noise and integration count. The noise is averaged by the movable mirror's integration count and is reduced to $1/\sqrt{N}$. Increasing the integration count increases the measurement time but increases the S/N.

[Figure 4-4] Noise characteristics (measurement example)

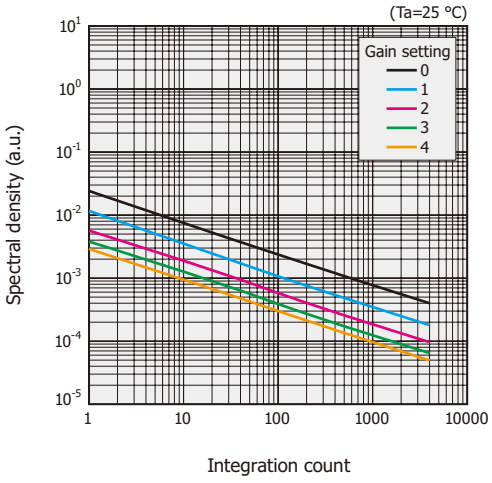

KACCB0610EA

4 - 2 Effects of optical fiber transmission loss

The output optical spectrum changes depending on the transmission loss characteristics of the optical fiber connected to the FTIR engine. A quartz fiber has a loss depending on the length of the optical fiber in the wavelength range longer than 2.1 µm. For this reason, a short optical fiber or fluoride fiber is recommended. Figure 4-6 shows the optical spectra when a fluoride fiber and quartz fibers of different lengths are used.

[Figure 4-5] Effects of optical fiber transmission loss

(a) Measurement system

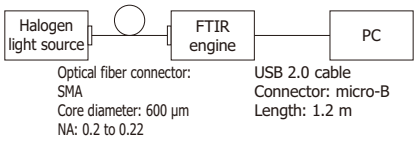

KACCC1020EA

(b) Optical spectra (measurement example)

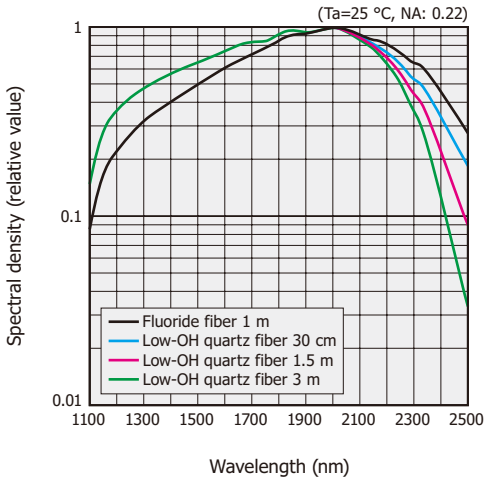

KACCB0611EA

4 - 3 Wavelength temperature dependence

Figure 4-7 shows the temperature characteristics of the peak wavelength and wavelength resolution (FWHM) of the laser spectrum measured by the FTIR engine in the measurement system shown in Figure 4-6. In this setup, a laser light (1532.8 nm) is input through an optical fiber, and the FTIR engine is placed in a constant temperature chamber. The FTIR engine is installed on a vibration isolation table to mitigate the effects of vibration in the constant temperature chamber.

[Figure 4-6] System for measuring temperature characteristics of wavelength accuracy and wavelength resolution

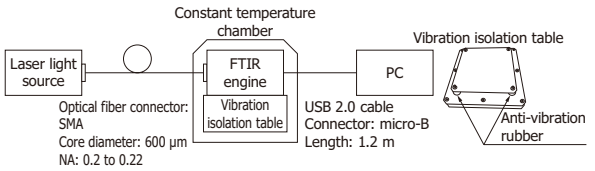

KACCC1021EA

[Figure 4-7] Wavelength temperature dependence (typical example)

(a) Peak wavelength

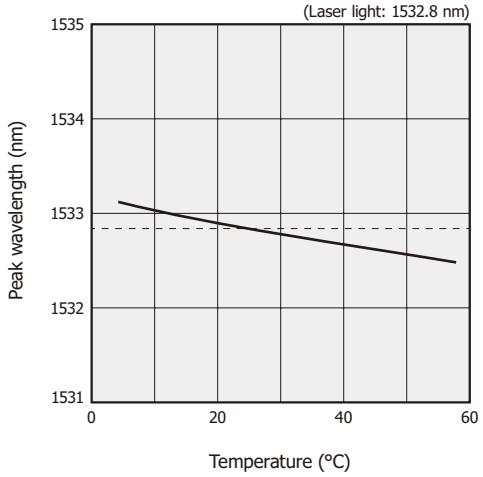

KACCB0612EA

(b) Spectral resolution

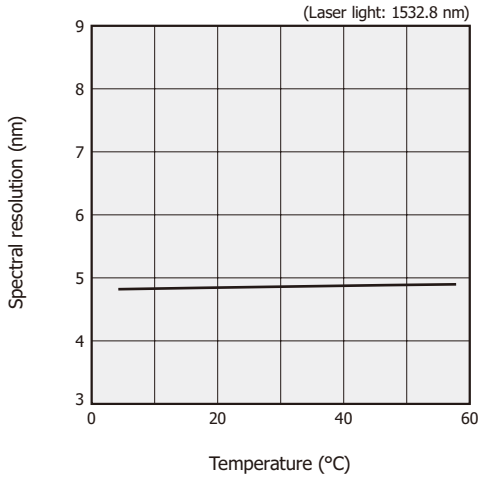

KACCB0613EA

The FTIR engine's wavelength temperature dependence depends on the oscillation wavelength of the VCSEL used to monitor the movable mirror. Since the VCSEL changes its oscillation wavelength depending on temperature, the wavelength accuracy measured by the FTIR engine has temperature characteristics. In Figure 4-7, the temperature measured by the thermistor in the FTIR engine when the temperature of the constant temperature chamber is changed is shown on the horizontal axis. The temperature inside the FTIR engine rises by about 5 °C due to the heat generated by the circuit driven by the FTIR engine. The peak wavelength of the laser spectrum detected by the FTIR engine shifts with temperature, and the wavelength temperature dependence is ±0.06 nm/°C or less. Note that the wavelength resolution (FWHM) is almost constant even when the temperature changes.

5. Measurement example

5 - 1 Absorption spectrum

In near-infrared spectroscopy, absorbance is calculated from the measured optical spectrum, and second derivative analysis, partial least squares (PLS) regression analysis, or the like is generally used. Absorbance is given by equation (5-1). Absorbance is also expressed by equation (5-2), and this is referred to as Lambert-Beer's law.

$$A\lambda = -\log_{10}(I_1/I_0) \cdots\cdots\cdots\cdots (5\text{-}1)$$

$A\lambda$: absorbance at wavelength λ
I_1 : transmitted light level
I_0 : incident light level

$$A\lambda = \alpha LC \cdots\cdots\cdots\cdots (5\text{-}2)$$

α: light absorption coefficient
L: optical path length of quartz cell
C: sample concentration

[Figure 5-1] Absorption spectrum measurement system

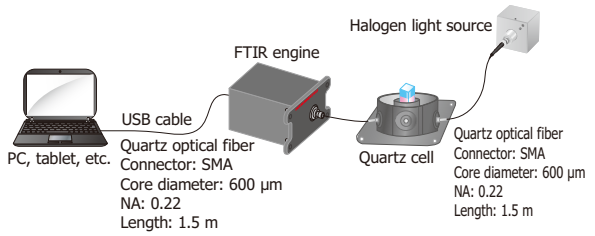

KACCC1022EA

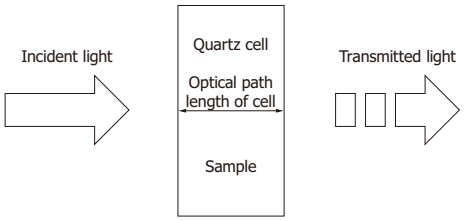

KACCC1023EA

Water

Figure 5-2 shows an example of a water absorption spectrum measurement by the FTIR engine in the measurement system shown in Figure 5-1. The absorbance changes according to the optical path length of the quartz cell. Absorbance is measured well up to about 2.

[Figure 5-2] Water absorption spectrum (measurement example)

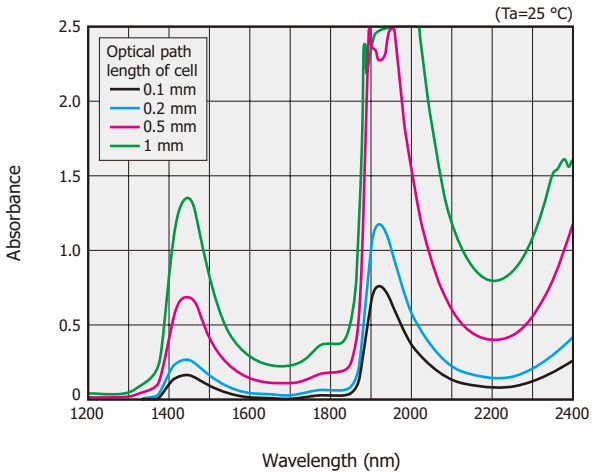

KACCB0614EA

Ethanol

Figure 5-3 shows a measurement example of the ethanol absorption spectrum. The ethanol absorption spectrum has a peak after 2200 nm. In this measurement, a zirconium fluoride (ZrF_4) fiber is used as the optical fiber for high sensitivity measurement in the long wavelength band (2100 to 2500 nm). Zero-fill processing is performed before the Fourier transform, and data points are interpolated to display a smooth spectrum.

[Figure 5-3] Ethanol absorption spectrum (measurement example)

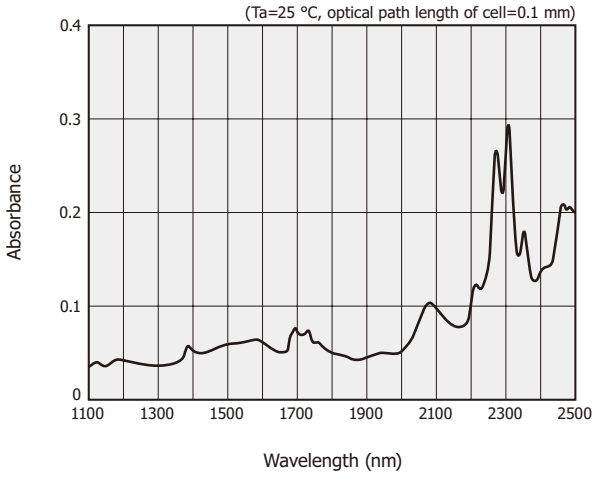

KACCB0616EA

Alcohols

Figure 5-4 shows the near-infrared absorption spectra of beer, sake, brandy, ethanol, and water. Absorption by water OH groups (1450 nm band, 1900 nm band) and absorption (2100 to 2500 nm) that differs depending on the molecular structure of the alcohol CH group exist. Absorbance is measured well in the range around 1 or 2.

Figure 5-5 shows an example of measuring the alcohol concentration from the absorbance in the 2260 nm band. Alcohol concentration and measured values are highly correlated.

[Figure 5-4] Absorption spectra of alcohols (measurement example)

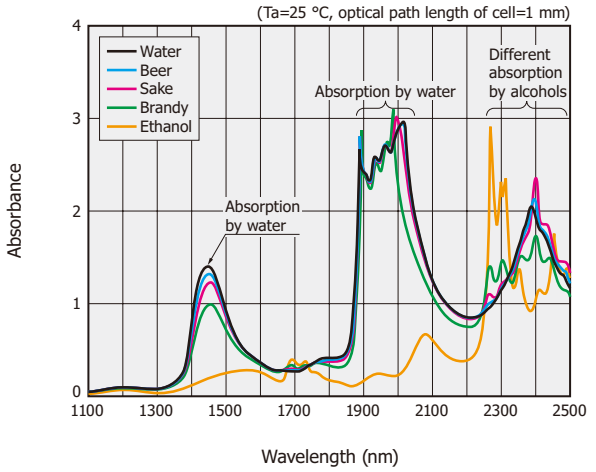

KACCB0622EA

[Figure 5-5] Concentration of alcohols (measurement example in 2300 nm band)

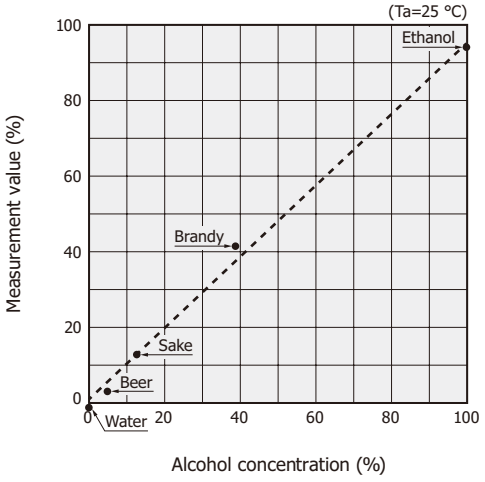

KACCB0623EA

Glucose

Figure 5-6 shows a measurement example of glucose concentration. Glucose concentrations are 0%, 0.2%, 0.4%, 0.8%, and 1%. Figure 5-6 shows the results of a PLS regression analysis based on absorbance data acquired for each concentration. The glucose concentration and measured values are highly correlated.

[Figure 5-6] Glucose concentration (measurement example in 1100 to 2500 nm band)

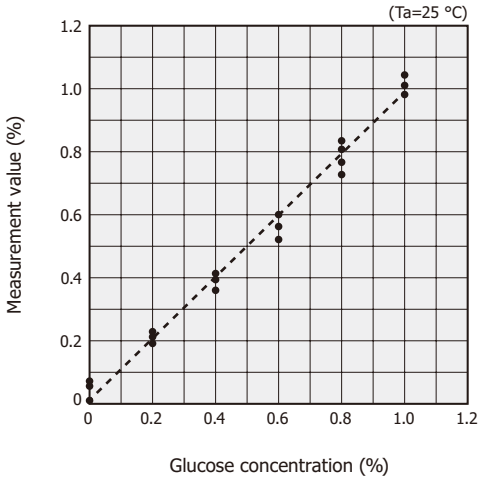

KACCB0615EA

5 - 2 Reflected light spectrum

Figure 5-7 shows the measurement system for the reflected light spectrum. A halogen light source is connected to a 6:1 reflection probe (a bundle of seven optical fibers: one at the center for receiving light, six at the periphery for irradiation), and light is incident on the FTIR engine. A reference plate is installed at the tip of the reflection probe, and the diffuse reflection light is measured by the FTIR engine.

[Figure 5-7] Reflected light spectrum measurement system

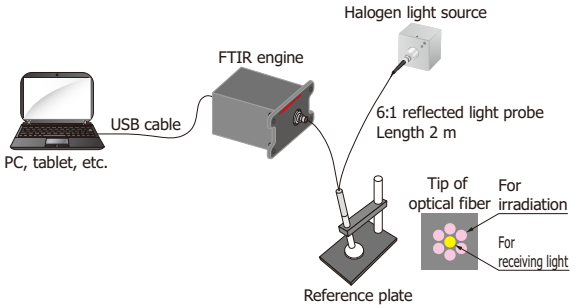

KACCC1024EA

Figure 5-8 shows a measurement example of white plastic (PP: polypropylene) containing brominated flame retardant. The absorption spectra due to the added compounds decabromodiphenyl ether (DBDE) and tetrabromobisphenol A (TBBA) are measured.

[Figure 5-8] Absorption spectra of white plastic containing brominated flame retardant (measurement example)

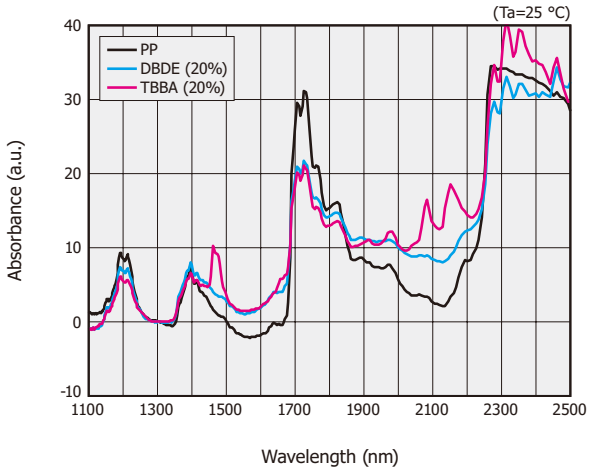

Data provided by Professor Kawazumi,
Faculty of Humanity-oriented Science and Engineering, Kindai University

KACCB0617EA

Figure 5-9 shows a measurement example of mortar material deterioration. Mortar materials are subjected to a freeze-thaw cycle of 8 hours in -15 °C and 4 hours in +30 °C, and absorbance spectra are measured to calculate the KM spectra. Three absorption bands are observed in the KM spectra before and after the freeze-thaw cycle. There are KM (≈absorbance) differences that are presumed to be due to the overtone of OH stretching vibration around 1450 nm, a combination of OH stretching and HOH bending around 1900 nm, and chloride ions around 2250 nm.

[Figure 5-9] Near infrared absorbance spectrum of mortar (measurement example)

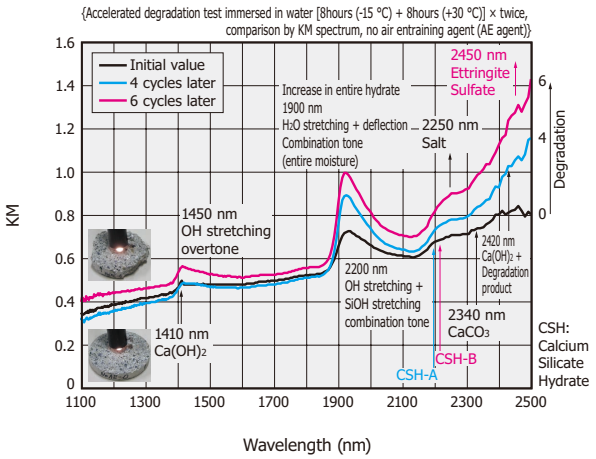

Schematic degradation reaction: $xCa(OH)_2 + ySiO_2 + nH_2O \rightarrow Ca_xSi_yO_{2y}(OH)_{2x} \cdot nH_2O$

CSH-A: Jennite-like: $Ca_9Si_6O_{18}(OH)_6 \cdot 8H_2O$

CSH-B: Tobermorite-like: $Ca_5Si_6O_{16}(OH)_2 \cdot 4H_2O$ or $Ca_5Si_6(O, OH)_{18} \cdot 5H_2O$

Data provided by Professor Nakajima, School of Science, Osaka University

KACCB0618EA

6. Vibration isolation table, evaluation software

6 - 1 Vibration isolation table

Since the FTIR engine is easily affected by vibration, a vibration isolation table is provided for stable measurement (sold separately). Anti-vibration gels are contained in the vibration isolation table to mitigate the effects of vibration. Mounting screws are used to secure the FTIR engine to the vibration isolation table.

6 - 2 Evaluation software

The data acquired by the FTIR engine is integrated and averaged by using the evaluation software supplied with the FTIR engine. The stability of the measurement differs depending on the selected integration mode [Table 6-1], but stable measurement is possible by using the vibration isolation table.

[Table 6-1] Integration mode

Integration mode	Features
0	The required data is transferred repeatedly to the PC (scan count). Fourier transform, integration, and averaging are performed repeatedly on the PC (scan count). This mode takes time but ensures stable measurements.
1	Integration and averaging are performed by the control circuit in the FTIR engine (scan count). The averaged data is transferred to the PC once, and Fourier transform is performed on the PC. This mode allows shorter measurements.

[Figure 6-1] Vibration isolation table with FTIR engine mounted

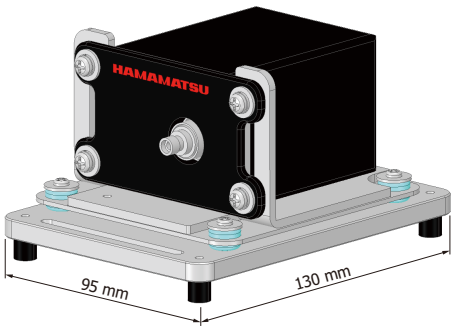

KACCC1025EA

Related information
www.hamamatsu.com/sp/ssd/doc_en.html

Precautions
· Disclaimer

Information described in this material is current as of May 2021.

Product specifications are subject to change without prior notice due to improvements or other reasons. This document has been carefully prepared and the information contained is believed to be accurate. In rare cases, however, there may be inaccuracies such as text errors. Before using these products, always contact us for the delivery specification sheet to check the latest specifications.

The product warranty is valid for one year after delivery and is limited to product repair or replacement for defects discovered and reported to us within that one year period. However, even if within the warranty period we accept absolutely no liability for any loss caused by natural disasters or improper product use.

HAMAMATSU

www.hamamatsu.com

HAMAMATSU PHOTONICS K.K., Solid State Division
1126-1 Ichino-cho, Higashi-ku, Hamamatsu City, 435-8558 Japan, Telephone: (81)53-434-3311, Fax: (81)53-434-5184

U.S.A.: Hamamatsu Corporation: 360 Foothill Road, Bridgewater, N.J. 08807, U.S.A., Telephone: (1)908-231-0960, Fax: (1)908-231-1218, E-mail: usa@hamamatsu.com
Germany: Hamamatsu Photonics Deutschland GmbH: Arzbergerstr. 10, D-82211 Herrsching am Ammersee, Germany, Telephone: (49)8152-375-0, Fax: (49)8152-265-8, E-mail: info@hamamatsu.de
France: Hamamatsu Photonics France S.A.R.L.: 19, Rue du Saule Trapu, Parc du Moulin de Massy, 91882 Massy Cedex, France, Telephone: (33)1 69 53 71 00, Fax: (33)1 69 53 71 10, E-mail: infos@hamamatsu.fr
United Kingdom: Hamamatsu Photonics UK Limited: 2 Howard Court, 10 Tewin Road, Welwyn Garden City, Hertfordshire AL7 1BW, UK, Telephone: (44)1707-294888, Fax: (44)1707-325777, E-mail: info@hamamatsu.co.uk
North Europe: Hamamatsu Photonics Norden AB: Torshamnsgatan 35 16440 Kista, Sweden, Telephone: (46)8-509 031 00, Fax: (46)8-509 031 01, E-mail: info@hamamatsu.se
Italy: Hamamatsu Photonics Italia S.r.l.: Strada della Moia, 1 int. 6, 20044 Arese (Milano), Italy, Telephone: (39)02-93 58 17 33, Fax: (39)02-93 58 17 41, E-mail: info@hamamatsu.it
China: Hamamatsu Photonics (China) Co., Ltd.: 1201 Tower B, Jiaming Center, 27 Dongsanhuan Beilu, Chaoyang District, 100020 Beijing, P.R.China, Telephone: (86)10-6586-6006, Fax: (86)10-6586-2866, E-mail: hpc@hamamatsu.com.cn
Taiwan: Hamamatsu Photonics Taiwan Co., Ltd.: 8F-3, No. 158, Section2, Gongdao 5th Road, East District, Hsinchu, 300, Taiwan R.O.C. Telephone: (886)3-659-0080, Fax: (886)3-659-0081, E-mail: info@hamamatsu.com.tw

Cat. No. KACC9012E02 May 2021 DN